JOURNAL OF GEOPHYSICAL RESEARCH, VOL. 89, NO. B12, PAGES 10,219–10,231, NOVEMBER 10, 1984

An Inhomogeneous Fault Model for Gaps, Asperities, Barriers, and Seismicity Migration

JOHN B. RUNDLE

Sandia National Laboratories, Albuquerque, New Mexico

HIROO KANAMORI

California Institute of Technology, Pasadena

KAREN C. MCNALLY

University of California, Santa Cruz

We develop a model for a fault in which various areas of the fault plane have different stress-slip constitutive laws. The model is conceptually simple, involving nonlinear algebraic equations which can easily be solved by a graphical method of successive iterations. Application is made to the problem of explaining seismicity patterns associated with great earthquakes. The model quantitatively explains phenomena associated with seismic gaps, asperities, and barriers.

1. INTRODUCTION

During the past few years a great deal of careful work by a variety of investigators has led to the conclusion that stress on fault planes is distributed in an inhomogeneous manner. For example, *Kanamori* [1981] and *Lay et al.* [1982] have documented seismicity data from around the world on major subduction plate boundaries and have shown that each area repeatedly exhibits a characteristic pattern of seismicity, which they believe is related to the existence of rough patches called asperities. *Lay et al.* [1982] also hypothesize that the geometric size of the asperities relative to their separation is what determines the failure mode of the subduction zone and also the characteristic seismicity pattern. Other work, involving waveform modeling [*Hartzell and Helmberger*, 1982; *Ebel and Helmberger*, 1982], has also demonstrated the probable existence of highly nonuniform stress distributions on fault planes, and in particular, *Hartzell and Helmberger* [1982] have used waveform modeling techniques to map out regions of nonuniformity on the fault plane during the Imperial Valley earthquake of 1979. In addition to these studies, other work has led to the conclusion that the seismicity patterns prior to and following great earthquakes can be classified into distinct patterns, including preseismic quiescence, precursory swarms, and doughnut patterns [*Mogi*, 1977; *McNally and Minster*, 1981; *Stewart et al.*, 1981; *Kanamori*, 1981; *Lay et al.*, 1982]. Foreshock migration inward toward the epicenter and aftershock migration away from the epicenter have also been observed [*Kagan and Knopoff*, 1976].

As a first step toward examining some of the basic physics inherent in processes associated with nonuniform stress distributions on fault planes, we formulate a simple model of a fault which allows different slip properties on different sections of the fault plane. The model consists of a circular fault embedded in an elastic material which is driven by boundaries at infinite distance which are translating at a uniform rate V_p. The fault is made up of rings with circular symmetry each of which has its own stress-slip constitutive law. Note that *McGarr* [1981] gives analytic expressions for the failure of a circular asperity within an annular faulted region. These expressions, however, are quite different from those derived here. By using an approximate solution for an annular region subjected to tensional stress, *McGarr* [1981] postulated a solution appropriate to an annular fault subjected to shear stress. This expression for the shear slip in the outer, annular region depends only on the level of shear stress in the outer, annular region. *McGarr* [1981] went on to apply this solution to the calculation of strong ground motion due to dynamic slip on the fault. By contrast, we find that the slip in the outer, annular region depends on the stress in both the outer, annular region as well as the stress in the inner, circular region. This general form can be shown to be correct from the linearity of the governing equations: the slip at a given point on the fault surface is a linear functional of the stress over the entire fault plane.

To find the solution to the problem in which the boundaries at infinite distance translate at uniform rate V_p, we superpose the solutions to a series of problems, two of which satisfy the equations of elastic equilibrium external to the fault plane. The other is a reasonable approximation to the solution of a general nonlinear viscoelastic problem representing steady slip at a plate boundary driven by mantle convection. The major assumption which is made in this procedure is that the far-field shear stress τ^∞ and the plate velocity V_p are bounded constants. Note that these two quantities cannot be specified independently, since they are related to each other through the physical processes which drive the plates as well as to internal inelastic deformation processes within the plate. Assuming that the plates are driven by mantle convection implies that τ_b, the basal shear stress on horizontal planes along the plate motion direction, is the nonzero, bounded stress ultimately producing the plate velocity V_p. The far-field shear stress in the plane of the fault, τ^∞, is then either the resolved component of τ_b in the plane of the fault (for subduction plate boundaries) or is produced from τ_b by inelastic deformation within the plate (for transform plate boundaries). We also assume that the plate responds elastically to incremental

Paper number 4B1030.
0148-0227/84/004B-1030$05.00

strains and stresses, thereby allowing use of singular dislocation solutions to describe deformation due to earthquakes at the plate boundary. Thus we speculate that this solution method can be viewed as a perturbation approach, in which the dislocation solutions represent a higher-order perturbation (small strain) on the lowest-order solution, steady slip. At the present time we cannot prove that a perturbation scheme like this exists for this problem or that it generates the correct solution, although we feel that it is certainly a reasonable approach.

Consistent with the above comments, we take the "lowest-order" solution to be uniform slip everywhere on the boundary $z = 0$ between two elastic half spaces, $z > 0$ and $z < 0$, at the slip velocity V_p. Since we are not interested in the absolute magnitude of the displacement of the plates from the beginning of time but only in the difference in displacement between two epochs, we will not be concerned with the details of stress and nonlinear strain within the plate. Uniform slip on the boundary at a rate V_p will produce uniform motion in the half space $z > 0$ of $0.5V_p$, and in the half space $z < 0$, of $-0.5V_p$. Note that for a linear elastic constitutive law, steady slip at the boundary together with bounded τ^∞ and V_p implies $\tau^\infty = 0$ for strike-slip plate boundaries. However, it is expected that the plate is characterized by a nonlinear constitutive relation between, say, Cauchy stress and some frame indifferent measure of deformation or deformation rate [*Truesdell and Noll*, 1965], so that the far field stress τ^∞ is produced from the basal shear stress τ_b. In any case, as will be seen later, the solution derived in this paper depends only on the difference between τ^∞ and the fault stress, so the absolute magnitude of τ^∞ is unimportant. That is, constitutive laws relating fault stress to slip, needed for complete solution of the problem, can in actual fact be regarded as constitutive laws relating relative stress to fault slip, since the far-field stress τ^∞ appears in the solution as an unconstrained parameter. Since the other solutions to be superposed on this one involve no other stresses or displacements at infinity, the stresses and velocities at infinity are then τ^∞ and $\pm 0.5V_p$ (the sign depending on the side of the plate boundary), as specified above.

The "perturbation" solutions to be superposed are solutions to dislocation problems. Suppose that we are given a compact surface Σ in the z plane, and suppose that we possess the solution $S(\delta)$ to a problem in which the slip δ on the surface Σ is specified and for which all displacements and stresses vanish in the far field at infinite distance from the surface. Let us now allow discrete episodes of slip to occur at the times $t_1, t_2, \cdots, t_n$, so that the variables $\delta(t_1), \delta(t_2), \cdots, \delta(t_n)$ define a history of slip on the fault in response to the plate velocity and stress pair τ^∞, V_p. These solutions, $S(\delta)$ and $S(-V_p t)$, when superposed upon the solution in the paragraph above, yield the solution to our problem. Practically speaking, the solution $S(\delta)$ turns out to be linear in δ, so that superposition of the second and third solutions yields $S(\delta - V_p t)$, where the δ are given. Note that upon the surface Σ, slip is zero between events, is $\delta(t_n)$ at time t_n, and accumulates a net offset at the rate V_p. Moreover, the stress and plate velocity at infinity are τ^∞, V_p as desired, since the two solutions $S(\delta)$ and $S(-V_p t)$ contribute no far-field perturbation stress or displacement for finite $\delta - V_p t$. Outside of the surface Σ but on the plane $z = 0$, the boundary is freely sliding at the rate V_p. If it is desired that the exterior region to Σ have stick-slip behavior, then it is necessary only to embed the fault within a larger fault, and so on.

The solution derived here in principle satisfies the governing differential field equations external to the slip surface, the boundary conditions at infinity, on the free surface $z = 0$, and on the surface Σ. We therefore postulate that this solution is "close" in some sense to the correct solution, given our uncertainty about permanent inelastic deformation within the plate. Since no uniqueness theorem is available for general inelastic materials, we cannot claim uniqueness: the lowest order solution, the steady state part of the total superposed solution, is clearly nonunique. However, the dislocation part of the total solution, $S(\delta - V_p t)$, is unique, given the assumption of incremental elasticity for the plate. This procedure has been used in the past to model cyclical earthquakes on both infinitely long strike-slip faults [*Savage and Prescott*, 1978] as well as infinitely long thrust faults [*Savage*, 1983; *Thatcher and Rundle*, 1984]. The justification given for its use was only that it seemed a reasonable method for calculating the deformation due to cyclic earthquakes on a fault.

It may be argued that simple models of this type have been superceded by more complex numerical models [*Stuart*, 1978, 1979; *Stuart and Mavko*, 1979]. However, it is our feeling that simple analytic models of the present type can provide a degree of physical insight not possible with much more complex models in which the interrelationships among the variables are not always intuitively clear. The advantages of computationally simple models such as these are clearly displayed as well by the simple spring-block slider model of an earthquake, still in common use by a variety of authors [*Cohen*, 1978; *Dieterich*, 1981, 1980]. Moreover, *McGarr* [1981] has shown that problems of this type can have important applications in calculating strong ground motion response to faulting.

In section 2 we solve the problem of a circular fault subjected to far-field stress τ^∞. In section 3 a solution technique is discussed which can be used to solve the governing equations by graphical perturbation, when an appropriate stress-slip constitutive law is given. Section 4 discusses the case of time periodic earthquakes and gives a pictorial illustration of the relationships between the field quantities. Section 5 shows some numerical calculations for synthetic earthquakes, assuming Mohr-Coulomb failure laws for a circular fault with two regions. Finally, section 6 discusses some applications, particularly to the October 1980 New Hebrides earthquakes.

Owing to the rather involved mathematical derivations in sections 2 and 3, the casual reader may want to skip these. In order to facilitate this mode the discussions in sections 1 and 4–7 have been made as self-contained as possible and make only minimal reference to the derivations. The central result of sections 2 and 3, which is used in the following discussions, can be found in equations (47) and (48). These relate the slip in the outer and inner regions of the circular fault to the stresses on the inner and outer regions.

2. MODEL

We start by considering an infinite linear elastic medium within which is embedded an ellipsoidal inclusion. The inclusion is supposed to be constructed of a material with elastic moduli different from the moduli of the surrounding material. For the case in which a general far-field stress is applied to the elastic medium, *Eshelby* [1957] derived the deformation within the inclusion by an elegant integration of the Green function for an elastic medium. His method is based upon finding the deformation everywhere within an elastic material from an "equivalent" inclusion which has been given a stress-

free transformation strain e_{ij}^T. Then, by application of boundary conditions the strain e_{ij}^T is found in terms of the applied far-field stress (or strain), the two sets of elastic moduli, and a shape factor S_{ijkl}. Thus the problem reduces to finding the deformation due to application of e_{ij}^T.

As a first step, consider the following sequence of operations [*Eshelby*, 1957]:

1. Make a cut over the ellipsoidal surface, remove the inclusion, and apply to it the uniform stress-free strain e_{ij}^T. At this stage it still has the elastic moduli λ, μ of the elastic medium. Thus

$$\sigma_{ij}^T = \lambda e^T \delta_{ij} + 2\mu e_{ij}^T \tag{1}$$

is the stress derived from e_{ij}^T by Hooke's law.

2. Apply surface tractions $-\sigma_{ij}^T n_j$ to the inclusion, bringing it back to the same size and shape it had prior to application of e_{ij}^T. Put it back in the elastic matrix and reweld the boundary S.

3. Let the surface tractions relax or, equivalently, apply a body force $+\sigma_{ij}^T n_j$ over the surface to cancel the surface traction applied in step 2. The medium is now in a state of self stress, and displacements everywhere are given by

$$u_i^C(\mathbf{r}) = \int_S dS_k \sigma_{jk}^T U_j(\mathbf{r} - \mathbf{r}') \tag{2}$$

where the elastostatic Green function U_j is given by

$$U_j(\mathbf{r} - \mathbf{r}') = \frac{1}{4\pi\mu} \frac{F_j}{|\mathbf{r} - \mathbf{r}'|} - \frac{1}{16\pi\mu(1-\nu)} F_1 \frac{(x_1 - x_1)(x_j - x_j)}{|\mathbf{r} - \mathbf{r}'|} \tag{3}$$

Here F_j is the magnitude of the point force in direction j.

In his classic paper, *Eshelby* [1957] shows that the "constrained strain" e_{ij}^C within the inclusion is uniform and is given by

$$e_{ij}^C = S_{ijkl} e_{kl}^T \tag{4}$$

where S_{ijkl} is a set of shape factors which depend on both the geometry of the inclusion and the elastic moduli. This problem, whose solution is outlined here, is often termed the equivalent inclusion because it holds the key to solving the following problem. Consider an ellipsoidal inclusion of the same shape and size but with moduli λ_1, μ_1, embedded in a matrix with moduli λ, μ which is subjected to a far-field stress σ_{ij}^∞. Since part of the strain in the equivalent inclusion problem is accomplished with zero stress, continuity of normal tractions yields

$$\kappa_1(e^c + e^\infty) = \kappa(e^c - e^T + e^\infty) \tag{5}$$

$$\mu_1('e_{ij}^c + 'e_{ij}^\infty) = \mu('e_{ij}^c - 'e_{ij}^T + 'e^\infty) \tag{6}$$

In (5)–(6) a backward prime denotes deviatoric strain, while no prime or indices denotes bulk strain. Bulk moduli κ, κ_1 have been used in (5). Equations (5)–(6) can now be solved to yield, for example [*Eshelby*, 1957],

$$e_{13}^T = \frac{\mu - \mu_1}{2(\mu_1 - \mu)S_{1313} + \mu} e_{13}^\infty \tag{7}$$

The normal strains $e_{11}^T, \cdots$, are not as easy to express and can in fact be found as the solutions to a set of coupled linear equations. It can be seen, then, that the shear stress-strain problem is decoupled from the normal stress-strain problem. In subsequent work we will make use of this property by considering only the application of shear stress in the direction parallel to a planar fault.

The solution to the entire problem is really based on the integral of the body force Green function $U_j(\mathbf{r} - \mathbf{r}')$ over the inclusion surface S. Of course, since the equations of elastostatic equilibrium are themselves linear, the response to a superposition of body forces is the superposition of the responses to the individual body forces. Hence we can define other surfaces, for example, inside the ellipsoidal surface of the inclusion and distribute body forces on them. This idea is the governing principle behind our inhomogeneous fault model.

Let us consider now the situation shown in Figure 1. Within an outer oblate spheroidal surface, the inclusion surface, lies an inner oblate spheroidal surface. The semimajor and semiminor axes of the ellipsoids are a_0, c, a_i, c, respectively. We will shortly allow both spheroids to flatten into planar disks in the plane $z = 0$, but at this point the shapes are not important. In terms similar to that of the *Eshelby* [1957] single inclusion problem outlined above, we adopt the following procedure:

1. Remove the outer ellipsoid, give it a stress-free strain $(e_{ij}^T)_o$, apply surface tractions $-(\sigma_{ij}^T)_o n_j$, replace it, and reweld. Note that at this stage the inner ellipsoid is removed along with the outer and is strained by the same amount.

2. Remove the inner ellipsoid, give it a stress-free strain $(e_{ij}^T)_i$, apply surface tractions $-(\sigma_{ij}^T)_i n_j$, replace it, and reweld.

We now specialize to the case where the inner and outer transformation strains $(e_{ij}^T)_o$, $(e_{ij}^T)_i$ have only the nonzero components

$$(e_{13}^T)_o = (e_{31}^T)_o \equiv e_o^T \tag{8}$$

$$(e_{13}^T)_i = (e_{31}^T)_i \equiv e_i^T \tag{9}$$

so that the only nonzero transformation stresses $(\sigma_{ij}^T)_o$ and $(\sigma_{ij}^T)_i$ are

$$(\sigma_{13}^T)_o = (\sigma_{31}^T)_o \equiv \sigma_o^T \tag{10}$$

$$(\sigma_{13}^T)_i = (\sigma_{31}^T)_i \equiv \sigma_i^T \tag{11}$$

We introduce the shorthand $L \equiv 2\mu$ and assume that in the far field, $z \to \infty$, the stress $\sigma_{13}^\infty = L\, e_{13}^\infty \equiv L\, e^\infty$ acts upon the infinite medium. Then the stress $\sigma_{13} \equiv \sigma_o^L$ in the outer ring is

$$\sigma_o^T = L(e_o^C + e^\infty - e_o^T) + 2L\, S_{1313}^L(R) e_i^T \tag{12}$$

where

$$e_o^C = 2S_{1313}^L e_o^T \tag{13}$$

from (4). In writing (12) we have implicitly assumed a coordinate system (x, y, z), where $r^2 = x^2 + y^2$ and $R^2 = r^2 + z^2$. The quantity $S_{1313}^L(R)$ expresses the influence of the inner ellipsoid upon its surroundings and in the far field behaves like $1/R^3$. The superscript L denotes use of the elastic moduli λ, μ in computing S_{1313}^L or $S_{1313}^L(R)$. This quantity is obtained by integrating the Green function (3) over the inner ellipsoidal surface, with the observation point outside the inner ellipsoid. The calculation of quantities of this type is described briefly by *Eshelby* [1957], *Kellogg* [1929], and *Routh* [1892]. In essence, it is necessary to perform integrals of the type

$$x\pi a_i^2 c \int_\lambda^\infty \frac{U(u)\, du}{(a_i^2 + u)\Delta} \tag{14}$$

where

$$\Delta = (a^2 + u)(c^2 + u)^{1/2}$$

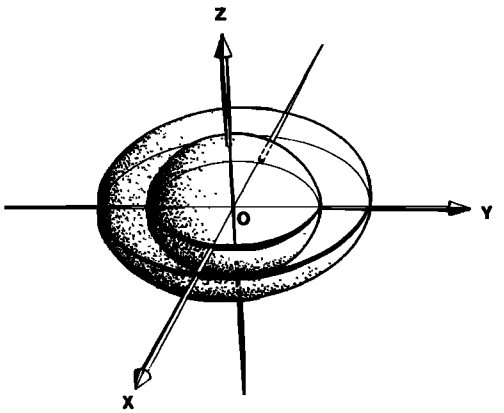

Fig. 1. An ellipsoidal sphereoid within an ellipsoidal sphereoid, the starting point of the model.

and where λ is the greatest positive root of the equation $U(u) = 0$:

$$U(u) = 1 - \frac{r^2}{(a_i^2 + u)} - \frac{z^2}{(c^2 + u)} \tag{15}$$

Integrals of the type (14) can be performed numerically since they die off as $u \to \infty$.

In the inner region the stress $\sigma_{13}{}^L \equiv \sigma_i{}^L$ is

$$\sigma_i{}^L = L(e_o{}^c + e_i{}^c + e^\infty - e_o{}^T - e_i{}^T) \tag{16}$$

where again

$$e_i{}^c = 2S_{1313}{}^L e_i{}^T \tag{17}$$

Having solved the equivalent inclusion problem, let us turn to the real problem of interest, in which inner and outer inclusions have different moduli, both from each other and from the matrix moduli. Hence

$$d\sigma_o{}^M/de_o \equiv M \tag{18}$$

$$d\sigma_i{}^N/de_i \equiv N \tag{19}$$

Also, let there exist corresponding Poisson's ratios ν_M and ν_N. At this point, we assume that both M and N are elastic shear moduli.

We now make two assumptions which considerably simplify the problem, allowing an analytic solution. The first assumption is that the inclusions are very flat, that is, $c/a_i \to 0$, $c/a_o \to 0$. The second is that $a_i \ll a_o$ (see Figure 2). The motivation for the second assumption is that when the inner ellipsoid is inserted into the outer ellipsoid, the influence function $S_{1313}{}^M(R)$ can be computed using the infinite space Green function, equation (3). To do the problem exactly would otherwise require the calculation of a correction term in the Green function corresponding to the modulus change across the outer ellipsoid boundary. Hence $S_{1313}{}^M(R)$ may be evaluated directly from the results given by *Eshelby* [1957] by replacing ν with ν_M and μ with $M/2$.

We therefore obtain the stress $\sigma_o{}^M$ inside the outer ellipsoid as

$$\sigma_o{}^M = M(e_o{}^c + e^\infty) + 2M\, S_{1313}{}^M(R) e_{i'}{}^T \tag{20}$$

The quantity $e_{i'}{}^T$ in general differs from $e_i{}^T$ in (12), (16)–(17) due to the modulus change in the outer ellipsoid. The stress inside the inner ellipsoid is

$$\sigma_i{}^N = N(e_o{}^c + e_{i'}{}^c + e^\infty) \tag{21}$$

Note that in (20)–(21), $e_o{}^c$ and $e_{i'}{}^c$ are defined as

$$e_o{}^c = 2S_{1313}{}^M e_o{}^T \tag{22}$$

$$e_{i'}{}^c = 2S_{1313}{}^M e_{i'}{}^T \tag{23}$$

Using the assumption that $c/a_i \to 0$, $c/a_o \to 0$, it can be shown that [*Eshelby*, 1957]

$$S_{1313}{}^L \to S_{1313}{}^M + 0(c/a_o) \tag{24}$$

$$S_{1313}{}^L \to S_{1313}{}^N + 0(c/a_i) \tag{25}$$

$$S_{1313}{}^L \to \frac{1}{8\pi} I_c + 0(c/a) \tag{26}$$

In (26), I_c is the integral

$$I_c = 2\pi \int_0^\infty \frac{dv}{(1+v)^2[(c^2/a^2) + v]^{1/2}} \to 4\pi \tag{27}$$

as $c/a \to 0$ and where $v = u/a^2$. We have used an unsubscripted a in (26) and (27) to denote either of (a_i, a_o).

As discussed previously, $S_{1313}{}^L(R)$, $S_{1313}{}^M(R)$, $S_{1313}{}^N(R)$ can be calculated by straightforward methods. However, we observe from the asymptotic forms of these quantities [*Eshelby*, 1957] that they die off proportional to $1/R^3$. Rather than compute numerically the exact values of $S_{1313}{}^L(R)$, $S_{1313}{}^M(R)$, $S_{1313}{}^N(R)$, we will thus simply use

$$S_{1313}{}^L(R) \to \frac{a_i{}^3}{2r^3} + 0\left(\frac{c}{a}\right) \qquad z = 0 \tag{28}$$

and so forth in expressions like (12), (20). This approximation should suffice at present in view of the nature of the model and the scatter in the data. Moreover, the final model will not use an R-dependent strain in the outer region but will rather use strain averaged over the ring area between the inner and outer disks. This approximation is made in a similar spirit to that of *Rice* [1979], who uses a crack solution with slip averaged over the area of the crack. Hence, except for what follows immediately, we shall replace $S_{1313}{}^L(R)$ by $\overline{S_{1313}{}^L}$

$$\begin{aligned}\overline{S_{1313}{}^L} &\equiv \left(\frac{1}{a_o{}^2 - a_i{}^2}\right) \int_{a_i}^{a_o} S_{1313}{}^L(R) R\, dR \\ &\approx \frac{a_i{}^3}{2}\left(\frac{1}{a_o{}^2 - a_i{}^2}\right) \int_{a_i}^{a_o} \frac{1}{r^2}\, dr \\ &= \frac{(a_i/a_o)^2}{2[1 - (a_i/a_o)]}\end{aligned} \tag{29}$$

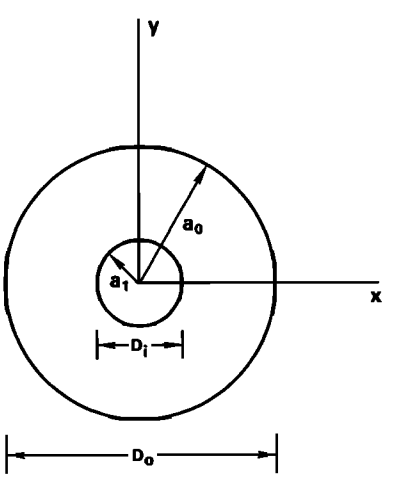

Fig. 2. Illustration of the circular fault plane, radius a_o, with a small circular patch, radius a_i.

For an asperity one third as large as the entire fault plane, $a_0 = 3a_i$, and (29) is about 0.08, a small number.

We now proceed with the remainder of the *Eshelby* [1957] formalism. Equating (12) and (20), and noting the R dependence of ${S_{1313}}^L(R)$, ${S_{1313}}^M(R)$, we obtain, to order c/a,

$$Me_{i'}{}^T = Le_i{}^T + 0(c/a_i) \tag{30}$$

$${e_o}^T = \frac{-(L-M)e^\infty}{2(L-M){S_{1313}}^L - L} + 0\left(\frac{c}{a_o}\right) \tag{31}$$

By equating (16) and (21), we find

$$[2(L-N){S_{1313}}^L - L]{e_o}^T + [2(M-N){S_{1313}}^L - M]e_{i'}{}^T + (L-N)e^\infty + 0(c/a_i) + 0(c/a_0) = 0 \tag{32}$$

Using (31), we obtain

$$e_{i'}{}^T = \frac{-L(N-M)e^\infty}{[2(L-M){S_{1313}}^L - L][2(M-N){S_{1313}}^L - M]} + 0\left(\frac{c}{a_i}\right) + 0\left(\frac{c}{a_o}\right) \tag{33}$$

and

$$e_i{}^T = \frac{-M(N-M)e^\infty}{[2(L-M){S_{1313}}^L - L][2(M-N){S_{1313}}^L - M]} + 0\left(\frac{c}{a_i}\right) + 0\left(\frac{c}{a_o}\right) \tag{34}$$

Let us define a quantity called the "ring strain" e_r equal to

$$e_r = {e_o}^c + e^\infty \tag{35}$$

We can then express $e_{i'}{}^T$ and $e_i{}^T$ as

$$e_{i'}{}^T = \frac{-(M-N)e_r}{[2(M-N){S_{1313}}^L - M]} \tag{36}$$

$$e_i{}^T = -\left(\frac{M}{L}\right)\frac{(M-N)e_r}{[2(M-N){S_{1313}}^L - M]} \tag{37}$$

It can be seen that (36) and (31) have exactly the same form: Each expresses the transformation strain in an inclusion as the same function of the corresponding elastic moduli multiplying the far-field strain of the medium in which it is embedded.

We now show that (31) can be reduced to an elementary, physically meaningful form. The expression for ${S_{1313}}^L$ can be reduced, in the limit $(c/a) \to 0$, to [*Eshelby*, 1957; *Rudnicki*, 1977]

$${S_{1313}}^L = \frac{1 - \xi(c/a)}{2} \tag{38}$$

where

$$\xi = \frac{3\pi(2-\nu)}{16(1-\nu)} \tag{39}$$

Using now a definition for far-field stress τ^∞ and one for fault stress τ_o

$$\tau^\infty = Le^\infty \tag{40}$$

$$\tau_o = Me_r \tag{41}$$

we find

$$\delta_r = \frac{\tau^\infty - \tau_o}{L}\frac{D_o}{\xi} \tag{42}$$

Here, D_o is the diameter of the fault (equals $2a_o$), and the fault slip δ_r is defined by

$$\tfrac{3}{2}\delta_r = {\delta_r}^{\max} \equiv 2ce_r \approx 2c{e_o}^c \approx 2c{e_o}^T \tag{43}$$

The equalities become exact as $c \to 0$. In reality, δ_r is an average fault slip in the sense of *Rice* [1979].

In a similar way, we find that the contribution to the slip in the central region δ_c from the transformation strain $e_i{}^T$ (not $e_{i'}{}^T$) is

$$\delta_c = \frac{\tau_o - \tau_i}{L}\frac{D_i}{\xi} \tag{44}$$

where

$$\tau_i = N(e_r + e_i{}^c) \tag{45}$$

$$\delta_c \equiv 2ce_i{}^T \tag{46}$$

and D_i is the diameter of the central region. Our final result, then, for the total slip in the inner part δ_i and outer part δ_o is

$$\delta_o = \frac{\tau^\infty - \tau_o}{L}\left(\frac{D_o}{\xi}\right) + 2\overline{S_{1313}}^L\frac{\tau_0 + \tau_i}{L}\left(\frac{D_i}{\xi}\right) \tag{47}$$

$$\delta_i = \frac{\tau^\infty - \tau_o}{L}\left(\frac{D_o}{\xi}\right) + \frac{\tau_o - \tau_i}{L}\left(\frac{D_i}{\xi}\right) \tag{48}$$

These are the equations to be solved for given τ^∞ and prescribed stress-slip constitutive laws between $\tau_o - \delta_o$ and $\tau_i - \delta_i$.

In defining constitutive laws for the fault stress-fault slip, we note, as does *Rice* [1979], that these laws of necessity incorporate the effects of distributed inelasticity in a region surrounding the fault plane. Moreover, slip on the fault plane is averaged in such a way that failure occurs simultaneously on every portion of the outer region and every portion of the inner region. Additionally, (47)–(48) are rather general in the sense that any deviations of these equations from the true governing equations can be "absorbed" into the stress-slip constitutive laws. For example, the $\tau - \delta$ constitutive law is assumed to incorporate the effects of changing normal stress on the fault plane as instability is approached. Thus constitutive laws determined from real seismicity data ought nevertheless to provide true insights into other independent data sets.

3. Solution by Successive Graphical Perturbations

Equations (47)–(48) are a set of nonlinear algebraic equations for δ_o and δ_i and can of course be solved numerically. However, note that the quantity $2\overline{S_{1313}}^L$ is a small number (call it $2\overline{S_{1313}}^L = \gamma \ll 1$). We can thus build upon a suggestion of *Rice* [1979], who noted that (42) can be solved graphically. Hence let us expand δ_o, δ_i, τ_o, and τ_i in powers of γ:

$$\delta_o = {\delta_o}^{(0)} + \gamma{\delta_o}^{(1)} + \gamma^2{\delta_o}^{(2)} + \cdots \tag{49}$$

$$\delta_i = {\delta_i}^{(0)} + \gamma{\delta_i}^{(1)} + \gamma^2{\delta_i}^{(2)} + \cdots \tag{50}$$

$$\tau_o = {\tau_o}^{(0)} + \gamma{\tau_o}^{(1)} + \gamma^2{\tau_o}^{(2)} + \cdots \tag{51}$$

$$\tau_i = {\tau_i}^{(0)} + \gamma{\tau_i}^{(1)} + \gamma^2{\tau_i}^{(2)} + \cdots \tag{52}$$

Inserting these expressions into (47)–(48) and collecting like powers of γ, we get at zeroth-order

$${\delta_o}^{(0)} = \frac{\tau^\infty - {\tau_o}^{(0)}}{L}\left(\frac{D_o}{\xi}\right) \tag{53}$$

$${\delta_i}^{(0)} = \frac{\tau^\infty - {\tau_o}^{(0)}}{L}\left(\frac{D_o}{\xi}\right) + \frac{{\tau_o}^{(0)} - {\tau_i}^{(0)}}{L}\left(\frac{D_i}{\xi}\right) \tag{54}$$

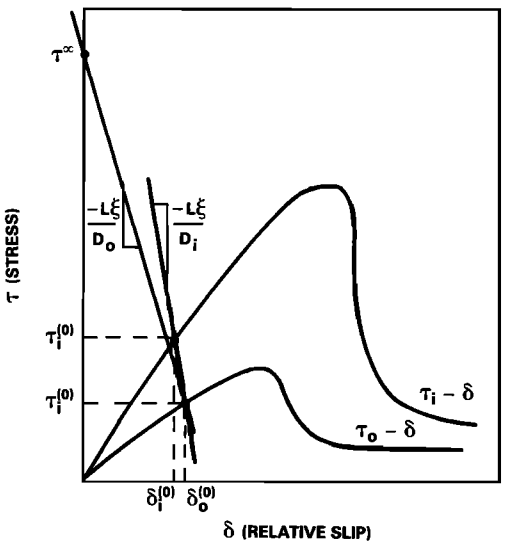

Fig. 3. Solution of Equations (47)–(48) by graphical construction. Two constitutive laws, for the outer regions $\tau_o - \delta$ and the inner region $\tau_i - \delta$, are shown together with lines constructed by use of the governing equations.

Equation (53) defines a line on the $\tau - \delta$ graph. Since τ^∞ is independent of δ, the line intercept is τ^∞, and slope is $-L\xi/D_o$. Notice that the slope, which is the effective stiffness, is directly proportional to the exterior shear modulus and inversely proportional to the diameter of the fault. The effective stiffness concept has been discussed in detail previously [*Walsh*, 1971]. Once $\tau_o^{(0)}$ has been defined, (54) defines a line on the $\tau - \delta$ graph with slope $-L\xi/D_i$ and intercept $\tau^\infty(D_o/D_i) + \tau_o^{(0)}(1 - D_o/D_i)$. Note that the magnitude of this second slope is larger than the slope of the line (53) because $D_o > D_i$.

As an illustration of the solution of the zeroth-order equations (53)–(54), we show in Figure 3 two curves in the $\tau - \delta$ plane representing stress in the inner and outer regions. We assume for the moment that the inner region can support a greater magnitude of shear stress than can the outer region. The two lines represented by (53)–(54) are shown with slope $-L\xi/D_o$ and $-L\xi/D_i$. The intersection of the first line with the vertical axis defines τ^∞, and the intersection with the $\tau_o - \delta$ curve defines both $\tau_o^{(0)}$ and $\delta_o^{(0)}$. From the intersection with the $\tau_o - \delta$ curve a line is drawn with slope $-L\xi/D_i$. Where it intersects the $\tau_i - \delta$ curve it defines $\tau_i^{(0)}$ and $\delta_i^{(0)}$.

We now retain terms of first order in γ in the solution expansion. Equations (47)–(48) become

$$\delta_o^{(0)} + \gamma\delta_o^{(1)} = \frac{\tau^\infty - (\tau_o^{(0)} + \gamma\tau_o^{(1)})}{L}\left(\frac{D_o}{\xi}\right) + \gamma\left(\frac{\tau_o^{(0)} - \tau_i^{(0)}}{L}\right)\left(\frac{D_i}{\xi}\right) \quad (55)$$

$$\delta_i^{(0)} + \gamma\delta_o^{(1)} = \frac{\tau^\infty - (\tau_o^{(0)} + \gamma\tau_o^{(1)})}{L}\left(\frac{D_o}{\xi}\right) + \left(\frac{(\tau_o^{(0)} + \gamma\tau_o^{(1)}) - (\tau_i + \gamma\tau_i^{(1)})}{L}\right)\left(\frac{D_i}{\xi}\right) \quad (56)$$

Defining

$$\bar{\delta}_o^{(1)} \equiv \delta_o^{(0)} + \gamma\delta_o^{(1)} \quad (57)$$

$$\bar{\delta}_i^{(1)} \equiv \delta_i^{(0)} + \gamma\delta_i^{(1)} \quad (58)$$

$$\bar{\tau}_o^{(1)} \equiv \tau_o^{(0)} + \gamma\tau_o^{(1)} \quad (59)$$

$$\bar{\tau}_i^{(1)} \equiv \tau_i^{(0)} + \gamma\tau_i^{(1)} \quad (60)$$

we obtain

$$\bar{\delta}_o^{(1)} = \frac{\tau^\infty - \bar{\tau}_o^{(1)}}{L}\left(\frac{D_o}{\xi}\right) + \gamma\left(\frac{\tau_o^{(0)} - \tau_i^{(0)}}{L}\right)\left(\frac{D_i}{\xi}\right) \quad (61)$$

$$\bar{\delta}_i^{(1)} \equiv \frac{\tau^\infty - \bar{\tau}_0^{(1)}}{L}\left(\frac{D_o}{\xi}\right) + \left(\frac{\bar{\tau}_o^{(1)} - \bar{\tau}_i^{(1)}}{L}\right)\left(\frac{D_i}{\xi}\right) \quad (62)$$

Note that we can transform the second term in (61) by use of (53)–(54) so that (61) reads

$$\bar{\delta}_o^{(1)} = \frac{\tau^\infty - \bar{\tau}_o^{(1)}}{L}\left(\frac{D_o}{\xi}\right) - \gamma(\delta_o^{(0)} - \delta_i^{(0)}) \quad (63)$$

Defining

$$\bar{\delta}_o^{(0)} \equiv \bar{\delta}_o^{(1)} + \gamma(\delta_o^{(0)} - \delta_i^{(0)}) \quad (64)$$

we have the same equations for $\bar{\delta}_o^{(1)}$, $\bar{\delta}_i^{(1)}$, $\bar{\tau}_o^{(1)}$, $\bar{\tau}_i^{(1)}$ as we had before, equations (53)–(54). Hence it can be seen that the next higher-order estimate of the total slip δ_o in the outer ring is $\delta_o^{(0)}$ reduced by the small quantity $\gamma(\delta_o^{(0)} - \delta_i^{(0)})$. The inner slip $\bar{\delta}_i^{(1)}$ is also then reduced by a small quantity of order δ. The same graphical construction, as was used for $\delta_o^{(0)}$, $\delta_i^{(0)}$, will thus suffice to determine δ_o, δ_i at first order.

The general form for the nth order equations is

$$\bar{\delta}_o^{(n)} = \frac{\tau^\infty - \bar{\tau}_o^{(n)}}{L}\left(\frac{D_o}{\xi}\right) + \gamma\left(\frac{\bar{\tau}_o^{(n-1)} - \bar{\tau}_i^{(n-1)}}{L}\right)\left(\frac{D_i}{\xi}\right) \quad (65)$$

$$\bar{\delta}_i^{(n)} = \frac{\tau^\infty - \bar{\tau}_o^{(n)}}{L}\left(\frac{D_o}{\xi}\right) + \left(\frac{\bar{\tau}_o^{(n)} - \bar{\tau}_i^{(n)}}{L}\right)\left(\frac{D_i}{\xi}\right) \quad (66)$$

As noted above, (65) can also be written as

$$\bar{\delta}_o^{(n)} = \frac{\tau^\infty - \bar{\tau}_p^{(n)}}{L}\left(\frac{D_o}{\xi}\right) - \gamma(\bar{\delta}_o^{(n-1)} - \bar{\delta}_i^{(n-1)}) \quad (67)$$

Hence the slip δ_o, δ_i in the outer and inner portions of the fault can be determined at successively higher orders by graphical construction. Note that the quantity $\bar{\delta}_o^{(n)} - \bar{\delta}_i^{(n)}$ is negative for a central region which can support a higher stress than the ring region. In the current seismological jargon this model is termed an asperity model. It can thus be concluded that the stronger asperity inhibits slip in the weaker region surrounding it by acting rather like a nail holding the two sides of the fault together.

Higher levels of complexity in the fault model can also be modeled by similar techniques to those used here. For example, if there exist regions with different $\tau - \delta$ properties such that $D_1 \ll D_2 \ll D_3$, we can write

$$\delta_3 = \frac{\tau^\infty - \tau_3}{L}\left(\frac{D_3}{\xi}\right) + \gamma_2\left(\frac{\tau_3 - \tau_2}{L}\right)\frac{D_2}{\xi} + \gamma_1\left(\frac{\tau_2 - \tau_1}{L}\right)\left(\frac{D_1}{\xi}\right) \quad (68)$$

$$\delta_2 = \frac{\tau^\infty - \tau_3}{L}\left(\frac{D_3}{\xi}\right) + \left(\frac{\tau_3 - \tau_2}{L}\right)\frac{D_2}{\xi} + \gamma_1\left(\frac{\tau_2 - \tau_1}{L}\right)\left(\frac{D_1}{\xi}\right) \quad (69)$$

$$\delta_1 = \frac{\tau^\infty - \tau_3}{L}\left(\frac{D_3}{\xi}\right) + \left(\frac{\tau_3 - \tau_2}{L}\right)\frac{D_2}{\xi} + \left(\frac{\tau_2 - \tau_1}{L}\right)\left(\frac{D_1}{\xi}\right) \quad (70)$$

where γ_1 is $2S_{1313}{}^L(R)$ averaged over the region from $D_1/2$ to $D_3/2$ and γ_2 is $2S_{1313}{}^L(R)$ averaged from $D_2/2$ to $D_3/2$. The

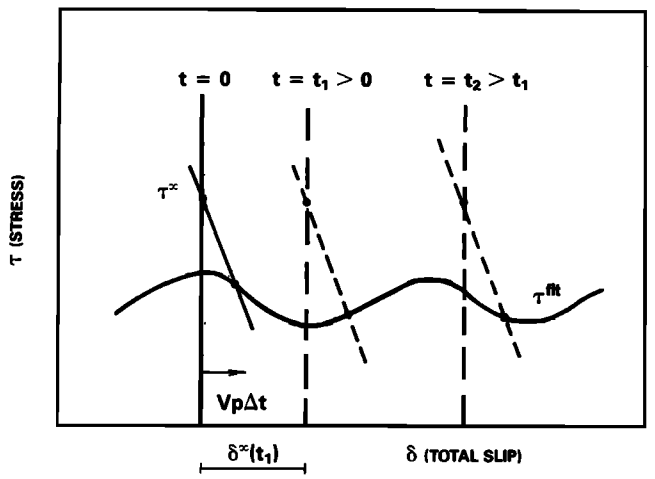

Fig. 4. Illustration of graphical solution to homogeneous fault problem when far-field stress τ^∞ is constant and far-field displacement δ^∞ increases monotonically with time. Fault stress is always less than τ^∞, and constitutive law is relatively flat so only quasi-static slip results.

same kind of solution method based upon graphical perturbation can be devised for (68)–(70) as was used for (47)–(48). With this kind of model it should be possible to analyze data quantitatively, indicating a migration of seismicity toward the eventual mainshock epicenter prior to the mainshock and migration of seismicity away from the event.

4. Time Periodic Earthquakes

For the remainder of this paper we take as our starting point (47) and (48). In these two equations the quantity L is twice the shear modulus μ; D is the diameter of the circular fault, with subscript o or i denoting outer or inner parts of the fault shown in Figure 2; ξ is given as a function of Poisson's ratio ν by (39); and $2\overline{S_{1313}}^L$ is a small quantity given by (29) in terms of the inner and outer radii of the circular faults a_i, a_o. The quantities δ_i, δ_o are the slip on the inner and outer parts of the fault, and τ_i, τ_o are the fault stresses on the inner and outer parts of the fault.

The analysis in sections 2 and 3 has been based on the idea that far-field shear stress increases monotonically with time. Clearly, this leads to great difficulty after a long period of time, since the far-field shear stress becomes unbounded. As pointed out in section 1, the stress τ^∞ is ultimately derived from the basal stress driving the plate motion, and this must be a bounded constant. Hence we adopt the superposition scheme outlined in the introduction, whereby a steady state solution with slip on the plate boundary is combined with dislocation solutions. Therefore, as noted in the introduction, we need to replace the quantity δ in the dislocation solution (47)–(48) by the quantity $\delta - V_p t$. To obtain the complete motion to the problem of faulting on a plate boundary driven at a far field velocity V_p, we first solve (47) and (48) with δ replaced by $\delta - V_p t$, together with an appropriate constitutive law relating fault stress τ^{flt}, or relative stress $\tau^{flt} - \tau^\infty$, and slip δ. Then, the plate motion $V_p t$ is added to the calculated δ.

By using a variation on the graphical solution techniques discussed by *Rice* [1979] and in the previous section, we can illustrate the solution as in Figures 4 and 5. Again, we note that equations in the form of (53) plot as straight lines on $\tau - \delta$ graphs, with stress intercept equal to τ^∞, and with slope $-L\xi/D_o$. If on the same graph, we plot the $\tau^{flt} - \delta$ constitutive law (the wavey line), then the intersection of the former line with the latter curve determines the stress-slip state. For the case considered by *Rice* [1979] the vertical reference stress line, upon which τ^∞ is located, is fixed at the left side. As the far-field stress increases in the *Rice* [1979] model, the stress intercept increases at some steady rate. However, in the present case the far-field displacement $V_p t$ increases steadily with time, and this can be represented by allowing the reference line to move steadily to the right at a velocity V_p. Hence the reference line is in the positions indicated at t_1 and t_2. As the reference line advances to the right, failure occurs when the slope of the $\tau^{flt} - \delta$ curve exceeds the slope of the elastic unloading line. This is precisely as before, only now the time-dependent fault slip has been placed in the context of a changing far-field reference state.

Figure 4 shows a case involving peak fault stress $\tau_p{}^{flt}$ lower than far-field stress τ^∞. In addition, Figure 4 also shows the case where the slope of the fault constitutive law always exceeds the slope of the elastic unloading line, so that only stable slip can occur. By contrast, Figure 5 shows a case in which the peak fault stress $\tau_p{}^{flt}$ exceeds the far-field stress τ^∞ and in which the slope of the elastic unloading line sometimes exceeds the slope of the constitutive law, thereby allowing unstable slip. *Rice* [1979] has called this the "seismic gap" model for the uniform fault. As the reference line advances to the right following $t = 0$, the fault slip begins to fall behind the far-field plate motion, whose position is represented by the position of the reference line. At $t = t_2$ the slope of the elastic unloading line exceeds the slope of the fault constitutive law, and failure occurs. The immediate prefailure stress-slip state δ_{pre} at peak stress is succeeded by the immediate postfailure stress-slip state indicated as δ_{post}. Hence, an "overshoot" of the reference state, represented as the position of the reference line, occurs during the earthquake.

It is worthwhile comparing the properties of the stress-slip constitutive laws of Figures 3–5 to the results of the friction experiments of *Dieterich* [1979]. Dieterich showed that frictional force depends inversely on slip velocity, being greatest when velocity is least and vice versa. However, this dependence has a certain "displacement lag" associated with it, in that friction changes to its lower (or higher) value only after a certain characteristic slip distance d_o has been traversed. This

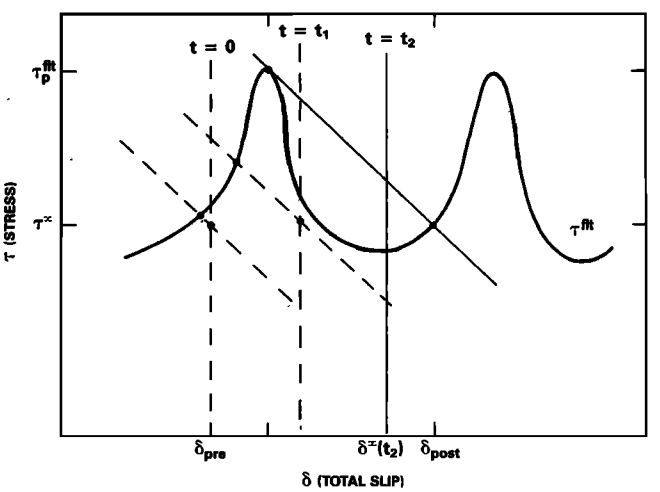

Fig. 5. Similar to Figure 4, only now fault stress is sometimes greater than far-field stress τ^∞, and constitutive law is sharply peaked. Hence sudden fault rupture (earthquakes) can occur.

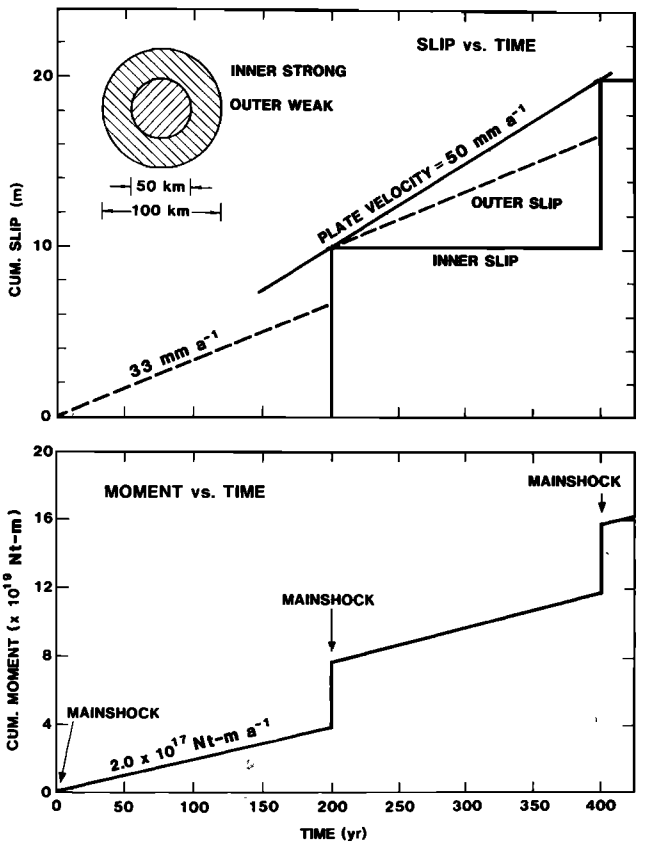

Fig. 6. Cumulative slip versus time and cumulative moment versus time during a steady state earthquake cycle for fault shown in the upper left corner.

constant d_o is in effect the distance which must be slipped to change the population of contacts between the two sides of the fault. The constitutive laws shown in Figures 4–5 also have a characteristic distance associated with them, the distance between the stress peaks. The similarity ends there, however. *Dieterich*'s [1979] evolutionary frictional laws are in reality a set of coupled, nonlinear partial differential equations. These show that frictional force is fundamentally rate dependent. It is easy to incorporate these frictional laws into the formalism developed here, by solving (47)–(48) for the ratio of shear to normal stress. Equating to *Dieterich*'s [1979] coefficient of friction and using the evolution equation for asperity contact time, we are left with a set of four nonlinear coupled partial differential equations to solve. Although this problem is not considered further here, we intend to pursue this in future work.

Finally, we note that earthquake stress drops, $\Delta\tau^{fu}$, divided by fault offset $\Delta\delta$ is an observational means of obtaining the slope of the elastic unloading line. This slope, equal to $-L\xi/D$, can be used to find any of the three quantities L, ξ, or D if the other two are assumed known. For example, one value of ξ is given in (39) for the circular fault problem. Another, given by *Rice* [1979] for the infinitely long fault, where D is then the width of the fault plane, is equal to $2/[\pi(1-\nu)]$. Other geometries will have different interpretations of D and ξ.

5. Synthetic Earthquakes

As a first step in the generation of synthetic earthquakes for elucidation of the physics of real events, we assume a simple Mohr failure criterion. Stress is allowed to increase on the fault with no associated displacement, until a peak stress τ^P is achieved. At this point, further far-field stress or displacment increase tends to cause fault stress to exceed τ^P, which is not allowed. Hence an earthquake is the result, with associated fault slip δ_f. In our simple model (Figure 2) we need to specify peak stresses τ_o^P, τ_i^P, and event slip δ_f^o and δ_f^i for both the inner and the outer regions.

To solve the system of (47)–(48) subject to Mohr constitutive laws, it is convenient to invert (47)–(48) and solve for stress as a function of slip. Thus we have

$$\tau_o = A_1\delta_o + A_2\delta_i + A_3\delta^\infty + \tau^\infty \tag{71}$$

$$\tau_i = B_1\delta_i + B_2\delta_o + B_3\delta^\infty + \tau^\infty \tag{72}$$

where

$$\begin{aligned} A_1 &= \frac{-2\mu\xi}{D_o(1-\gamma)} \\ A_2 &= \frac{2\mu\xi\gamma}{D_o(1-\gamma)} \\ A_3 &= 2\mu\xi/D_o \\ B_1 &= \frac{2\mu\xi(\gamma D_i - D_o)}{D_iD_o(1-\gamma)} \\ B_2 &= \frac{2\mu\xi(D_o - D_i)}{D_iD_o(1-\gamma)} \\ B_3 &= 2\mu\xi/D_o \\ \delta^\infty &= V_{pl}t \\ \gamma &= 2\overline{S_{1313}}^L \end{aligned} \tag{73}$$

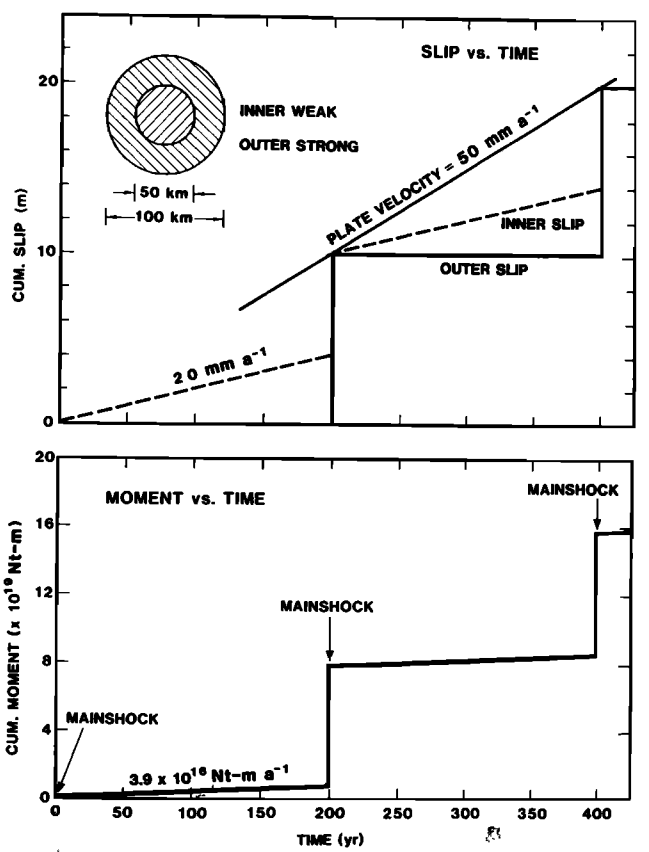

Fig. 7. Cumulative slip versus time and cumulative moment versus time during a steady state earthquake cycle for fault shown in the upper left corner.

Equations (71)–(72) are in fact extremely revealing. They show that slip on one region of the fault plane tends to "trigger" slip on the other. That is, A_1 is negative, so that slip on the outer part reduces stress on the outer part. However, since A_2 is positive, slip on the inner part increases stress on the outer part. Likewise, since $B_1 < 0$ and $B_2 > 0$, slip on the inner part reduces stress on the inner part, but slip on the outer part increases stress on the inner part.

In order to use (71)–(72) in a numerical algorithm, we set $\delta^\infty = V_P t$ and assume constant τ^∞. Let us also assume that we have some current value of slip δ_o', δ_i' on the fault plane. Also, (71)–(72) indicate that the only meaningful stress quantities are the stress differences $\tau_o - \tau^\infty$, $\tau_i - \tau^\infty$. It is these differences that we parameterized with the Mohr failure model, picking peak stresses τ_o^P, τ_i^P for each difference. We then compute the times to next failure T_o^f, T_i^f for each region

$$T_o^f = \frac{(\tau_o^P - A_1\delta_o' - A_2\delta_i')}{A_3 V_P} \tag{74}$$

$$T_i^f = \frac{(\tau_i^P - B_1\delta_i' - B_2\delta_o'}{B_3 V_P} \tag{75}$$

The shorter of T_o^f and T_i^f is then picked, time is incremented, the corresponding slip variable is incremented by δ_f^o or δ_f^i, and the procedure repeats. In the event that a large earthquake occurs, it is also necessary to check that the final stress state in each region is below the peak value. If it is not, either of δ_o' or δ_i' is incremented until that criterion is achieved.

The results of these calculations for selected examples are shown in Figures 6–9. All of these figures show, in the upper part, cumulative slip versus time, and, in the lower part, cumulative moment versus time. These plots are all for earthquake cycles once the system has reached a steady state. Shown in the upper left corner is a diagram of the fault plane. The outer ring has a diameter D_o of 100 km, whereas the inner circle can have a diameter D_i of either 50 or 25 km. Thus the physically important ratio $(D_i/D_o)^3$ is either 0.125 or 0.016. As illustrated in Figures 6–9, either region on the fault plane can be strong compared to the other or weak compared to the other. Also, as indicated, the far-field relative plate velocity has been assumed to be 50 mm/yr.

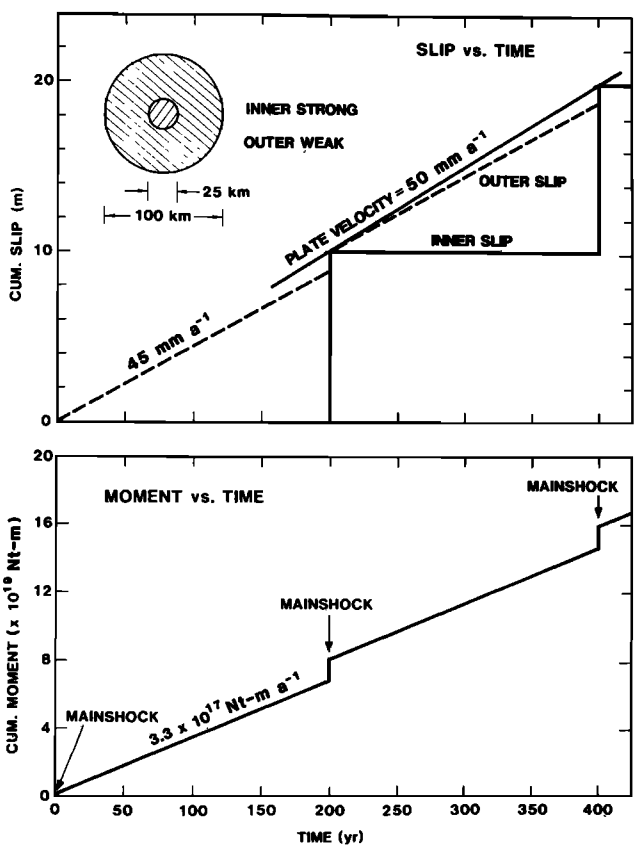

Fig. 8. Cumulative slip versus time and cumulative moment versus time during a steady state earthquake cycle for fault shown in the upper left corner.

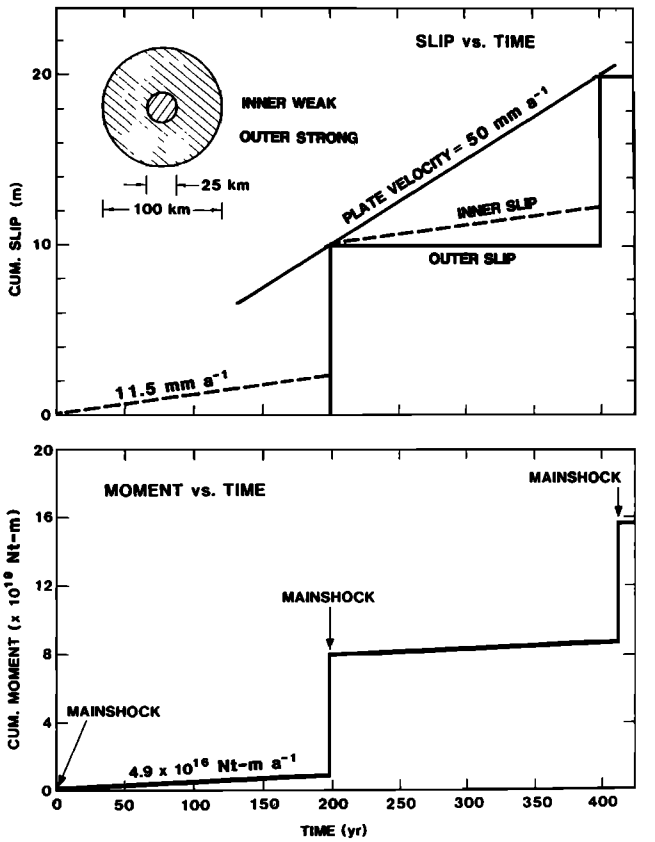

Fig. 9. Cumulative slip versus time and cumulative moment versus time during a steady state earthquake cycle for fault shown in the upper left corner.

The dashed line in the upper plot of Figures 6–9 is the cumulative slip occurring in the weaker portion of the fault plane. The solid, stair step line is the cumulative slip in the stronger portion of the fault plane. Slip accumulated during one cycle by the far-field plate motion is represented by the solid line connecting the two points of the stair step. The figures show the slip cycle after steady state has been achieved. During the "startup phase" of the model, the stress mismatch $\tau - \tau^\infty$ is adjusted by the system until the average slip rate on the fault matches the steady state far field displacement rate V_P. That all regions of a fault loaded at the same rate should display the same average total offset appears to be true of the San Andreas fault [*Weldon and Sieh*, 1981; K. E. Sieh and R. H. Jahns, unpublished manuscript, 1984].

In these synthetic earthquakes, the quantities δ_f^o and δ_f^i are taken to have the values 0.01 and 10 m, respectively. Note that cumulative outer slip and cumulative moment between large shocks have been drawn as straight lines rather than as the tiny, almost invisible, stair step functions they actually are. The physics underlying this simple Mohr constitutive law can

be understood in the context of *Dieterich*'s [1979] evolutionary friction law. Thus the quantity τ^P is the stress at which the velocity dependence (weakening) of the coefficient of friction commences. Use of a small value for $\delta_f{}^o$ then simply means that little or no friction decrease occurs with sliding; thus little unstable slip occurs. On the other hand, use of a large value for $\delta_f{}^i$ means that the coefficient of friction decreases greatly with the onset of slip, thereby allowing a large amount of unstable slip to occur during an event.

Figures 6–9 clearly demonstrate the existence of a triggering effect. Slip on the stronger region at $t = 200$, 400 years can be seen to trigger slip in the weaker region. The amount of triggered slip, plus the slip accumulated over the preceeding 200 years, just equals 10 m, the amount of displacement accumulated during that time by motion in the far field. Of course, the lower the rate of steady slip during the cycle, the higher is the amount of triggered slip. Triggering effects like this are now the focus of an increasing amount of interest [*Das and Aki*, 1977; *Dmowska and Li*, 1982; *Thatcher and Savage*, 1983].

6. APPLICATIONS

The applicability of the model described in the preceding sections can be demonstrated by reference to a number of studies of worldwide seismicity patterns. For example, *Mogi* [1968*a*, *b*] and *Tajima and Kanamori* [1981] have demonstrated that great subduction zone earthquake sequences often consist of one or more mainshocks, confined in a relatively small area, and an extensive aftershock sequence which expands from the mainshock area to fill a much larger region. *Lay et al.* [1982] have examined these patterns and classified them into a number of distinct categories. Some areas, such as Alaska and Chile, show little or no expansion of aftershock area over mainshock area and may represent faults with very uniform, strong slip surfaces. *Lay et al.* [1982] believe that these regions are essentially one big asperity. Other areas such as the Aleutians, which are characterized by some aftershock expansion, are hypothesized to represent regions with large, isolated discrete zones of strong slip surface coupling, i.e., the mainshock area or asperity. However, the size of the asperity is somewhat smaller than the region covered eventually by the aftershocks. A third category, exemplified by the Kurile Islands subduction zone, is also characterized by aftershock expansion but more importantly by complex source process for the mainshock and with several discrete source locations. *Lay et al.* [1982] hypothesize that this type of physical behavior reflects the lack of large isolated asperities and prefer instead a model with a distributed number of smaller, weaker asperities. The final category is typified by the Mariana subduction zone, in which no large earthquakes exist, hence no mainshock-aftershock patterns or expansion exist, and essentially all of the plate convergence is accommodated by aseismic slip.

A particularly good example of an isolated asperity appearing in the middle of an expanding aftershock region is shown by the October 1980 earthquake sequence near the Loyalty Islands, New Hebrides. Figure 10 shows data on this sequence developed by *Vidale and Kanamori* [1983]. A series of four mainshocks occurred which ranged in magnitude from $M_S = 6.5$ to $M_S = 7.2$, commencing at 0325 UT on October 24, 1980, and extending until October 25, 1980. The main shock epicentral locations were tightly clustered within the small dashed region in Figure 10 for the first 33–39 hours of the sequence. Activity subsequently spread over the region enclosed by the large dashed line in the 2400 hours following the main events. Obviously the asperity is represented by the area associated with mainshocks, and the total slip area is represented by the aftershock area.

It is to the picture of an isolated asperity embedded in the middle of an earthquake slip surface [e.g., *Lay et al.*, 1982, Figure 20] that we apply the model developed in preceding sections. Thus the central portion of the fault shown in Figure 2 is equated to the asperity region, the source of the mainshock. The outer ring of the fault shown in Figure 2 is then the region into which the aftershocks eventually expand. Last, the region exterior to the fault but in the same plane, which is considered in the model to be freely slipping (see the discussion in the introduction), approximates the effect of continued loading of the fault plane by events on the rest of the subduction zone. In using this model we equate the triggered slip, seen in Figures 6 and 8 on the "weaker," outer portion of the fault at the time of the mainshock, with the integrated slip due to all of the aftershocks. Obviously, the simple model application discussed in this paragraph does not treat a variety of physical phenomena which may occur in nature, such as preseismic quiescence, or foreshock clustering around the eventual mainshock area as exemplified by the Mogi doughnut. More geometrically complex models, in which more fault segments are considered, as well as use of the correct evolutionary constitutive laws would undoubtedly improve the situation. Moreover, inclusion of a layered earth structure with a free surface as well as stress relaxation in the asthenosphere through viscoelastic flow [*Rundle*, 1978; *Thatcher and Rundle*, 1979] is really necessary as well.

In Figure 11 we show the dependence of two slip ratios on normalized asperity size predicted from the model. The solid curve is the ratio of slip rate in the outer ring to plate velocity. Recalling the assumptions discussed above, we note that all of the slip in the asperity region is considered to be released during an earthquake cycle at the time of the mainshock. Hence we can alternately write this ratio as the ratio of the total moment in the aftershock region during the interval between mainshocks to the total moment of one mainshock sequence. The dashed line on Figure 11 represents the ratio of triggered slip due to aftershock occurrence to slip in the region of the asperity. Again, this curve can also be considered to be the ratio of total aftershock moment to total mainshock moment. Note that this identification of slip ratios with moment ratios depends critically on the assumption that little aseismic slip exists on the aftershock portion of the fault plane. This assumption is probably invalid in a number of subduction zones (see, for example, *Thatcher and Rundle* [1979, 1984] and Table 2 of *Lay et al.* [1982]). If, for any given time interval, background, mainshock, or aftershock, this proves to be a poor assumption, the corresponding moment calculated for that period will be too low. One common problem is probably neglect of very short term postseismic slip in both the mainshock and aftershock regions, so that plotted points would fall at too low an ordinate on Figure 11. Another problem is that the theoretical calculation models the effect of neighboring mainshock-aftershock sequences as simply steady slip at the background rate. This assumption means that short-term variations in the background slip rate and in the patterns of mainshock-aftershock sequences, due to large nearby events, are neglected. This assumption will affect the ordinates of plotted points in a nonsystematic way.

Using the ratio of moments approach, we have plotted points for several earthquakes on Figure 11. Events in the Marianas, where no large mainshocks occur, and in Alaska,

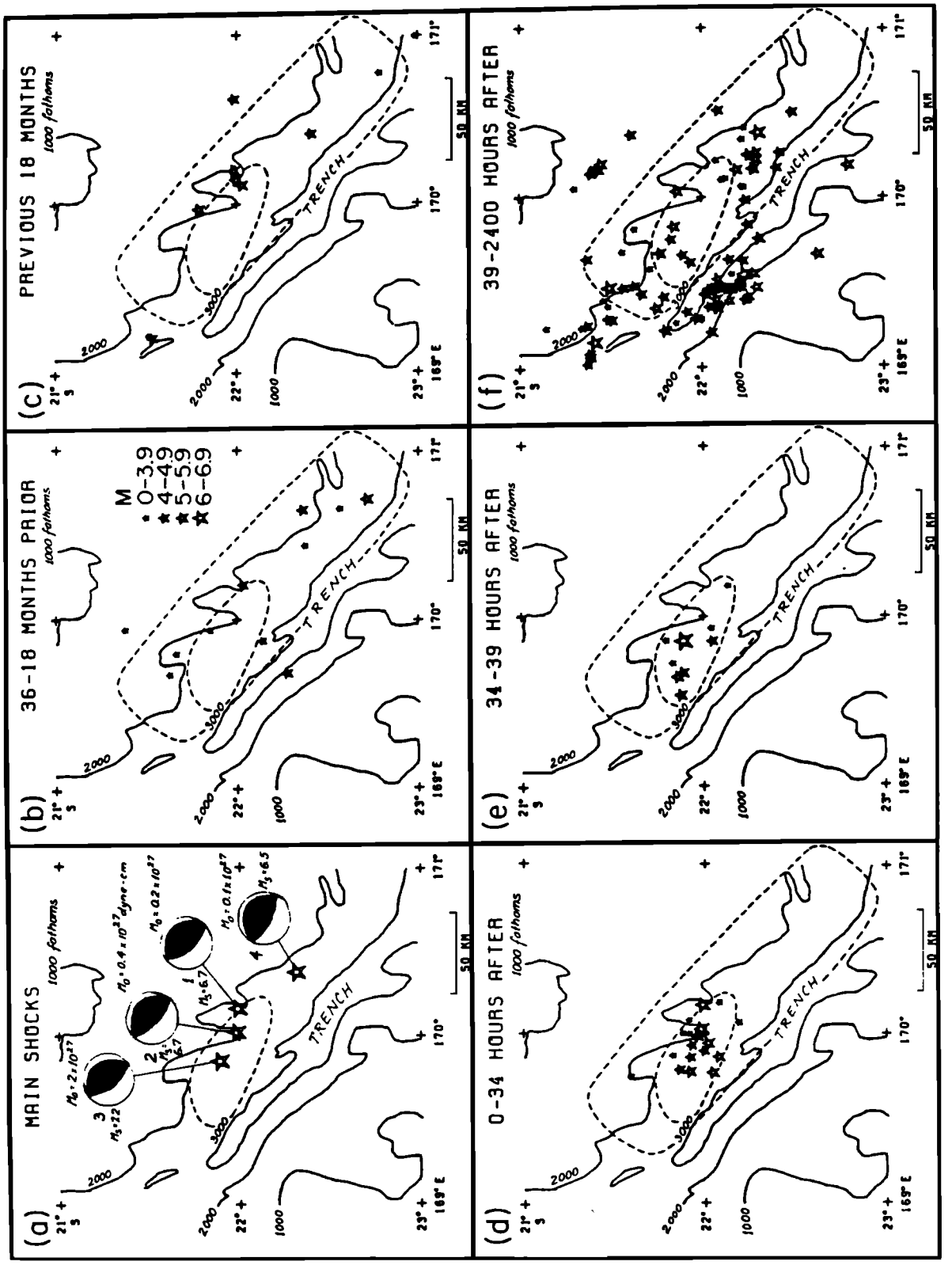

Fig. 10. Map showing mainshock–aftershock zones of the October 1980 Loyalty Islands earthquake sequence [from *Vidale and Kanamori*, 1983].

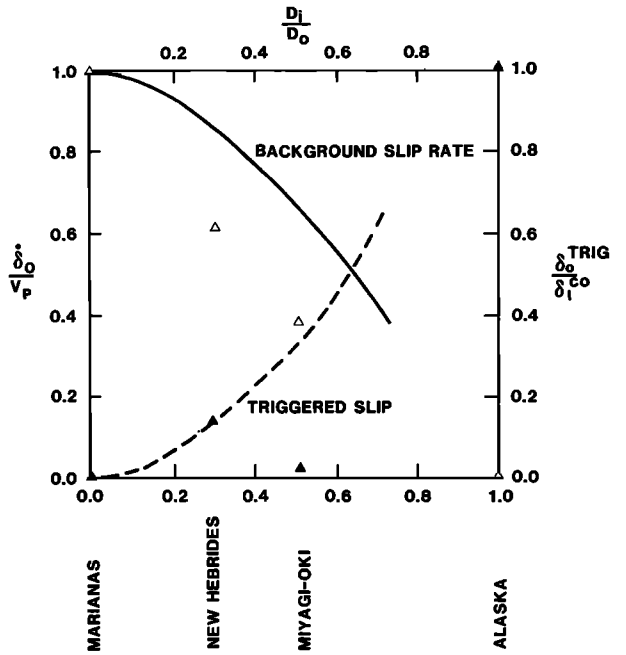

Fig. 11. Plot of normalized ring slip $\dot{\delta}_o/V_p$ and ratio of ring triggered slip δ_o^{trig} normalized by asperity slip $\delta_i^{\xi_o}$ as a function of relative asperity size. Points for various events (triangles) are plotted as described in the text. Solid triangles are for triggered slip or moment, and open triangles are for background slip rate or moment release.

where earthquakes occur as large, uniform ruptures with no aftershock expansion [*Lay et al.*, 1982], obviously represent limiting cases on Figure 11 and plot at the left-hand and right-hand margins as expected. More interesting cases are represented by the New Hebrides [*Vidale and Kanamori*, 1983], and Miyagi-Oki events [*Tajima and Kanamori*, 1981]. These two events, which are described below, both displayed some aftershock area expansion from the centrally located mainshock region, which indicates that they are probably characterized fairly well by the model of a uniform asperity embedded within a larger slip zone.

As described above, the October 1980 Loyalty Islands earthquake sequence involved a series of four mainshocks followed by a series of aftershocks extending over the 2400 hours following the main events, expanding to fill the area shown in Figure 10. In order to calculate the moment ratios discussed above we define three periods: period 1 is the "background period"; period 2 is the "coseismic period"; and period 3 is the "period of triggered slip". From the NOAA catalog we extracted all events larger than magnitude 5 which occurred within the box defined by the latitude-longitude vertices (−21.71°, 169.19°), (−21.29°, 169.58°), (−22.57°, 171.19°), (−23.00°, 170.73°). Since an $M_S = 7.25$ event occurred in this box on February 1, 1945, we consider the period from February 2, 1945, to October 23, 1980, to be the background period. The interval from October 24, 1980, to 1100, October 25, 1980, is then the coseismic period, and the period from 1100, October 25, 1980, to December 21, 1980, is the period of triggered slip. If we use the magnitude (M_S) moment (M_o) relation:

$$\log M_o = 1.5M_S + 16.1$$

then the total moment release for period 1 is 6.8×10^{19} N m; for period 2 is 1.1×10^{20} N m; and for period 3 is 1.3×10^{19} N m. The direct determination of the moment release for period 2 is 2.6×10^{20} N m [*Vidale and Kanamori*, 1983]. We assume that the moment determination for events in all three periods will display similar variation, and so we simply use the moments determined from the $M_S - M_o$ relation and the NOAA catalog. Using these values, the ratio of the moment for periods 1 to the ratio of the moment for period 2 is 0.02; and the ratio of the moment for period 3 to the moment for period 2 is 0.12. These are plotted in Figure 11 at the point corresponding to the ratio of asperity diameter to aftershock zone diameter characteristic of this region, 0.3. As can be seen, the ratio of background moment rate to plate convergence rate falls below the appropriate curve, while the ratio of triggered aftershock moment to mainshock moment falls on the theoretical curve.

In a manner similar to the Loyalty Islands earthquake we plot the data for the June 12, 1978, $M_S = 7.7$ Miyagi-Oki earthquake. This event occurred at a depth of about 40 km on a shallow-dipping fault and had a total aftershock expansion area of about 2400 km^2 [*Tajima and Kanamori*, 1981]. Repeat times in this area are about 100 years [*Lay et al.*, 1982], and the ratio of asperity diameter to aftershock zone diameter is about 0.5 [*Tajima and Kanamori*, 1981]. In order to calculate the total moment for the mainshock period and the period of triggered slip we take all events greater than magnitude 5 contained within the box bounded by the latitude-longitude vertices (38.8°, 141.9°), (38.2°, 143.8°), (37.2°, 143.2°), (37.8°, 141.2°). Using the moment magnitude relation above, we find that the mainshock moment is about 4.5×10^{20} N m and for the period of aftershock expansion, June 13, 1978, until May 31, 1982, the total moment is about 1.2×10^{19} N m. To find the ratio of mainshock moment to total background (interevent) moment, we must use the plate convergence rate in this area since no instrumental record of a prior mainshock for this area exists. Hence using the convergence rate of 0.1 m/yr [*Minster and Jordan*, 1978], together with an assumed shear modulus of 6.5×10^{10} N m^{-2}, the repeat time of 100 years, and the aftershock expansion area of 1800 km^2, we find a total background moment of 1.2×10^{21} N m. The ratio of moments then becomes 0.38 for period 2 to period 1 and 0.03 for period 3 to period 2. As can be seen on Figure 11, both points for the Miyagi-Oki event fall below their appropriate curves, indicating the possible presence of appreciable aseismic slip during the various periods.

Although we will not explore the question in any detail, it is also possible that mainshock m_b/M_S should vary predictably with D_i/D_o, background activity rate, the degree of aftershock expansion, and moment release of aftershocks. The justification for this suspected relationship is the idea that m_b is related to asperity size, while M_S is related to total fault area, including aftershock area [*Lay et al.*, 1982]. We also speculate that stress drops in events of a given region may display greater consistency if proper account is taken of relative sizes of asperity to total fault area. The ratio of stress drop on the asperity to stress drop over the aftershock ring may then be related to m_b/M_S as well as the other quantities mentioned above.

As mentioned above, the kinematics of the system appear to control the interevent recurrence time. Also, the recurrence time at a particular location is dependent on triggering effects from slip on nearby fault segments whose influence "diffuses" gradually along the fault. This is shown by reference to Figures 6–9. During the interval between mainshocks, activity on the outer ring, say, of Figures 6 and 8, occurs at a steady, predictable rate and is both slip and time predictable in the sense of *Shimazaki and Nakata* [1980]. However, when slip on a neighboring segment such as the asperity occurs, this simple

relationship is destroyed, and activity in the outer ring is elevated to a new time or slip predictable asymptote. Hence a simple time or slip predictable model is not valid for segments in fault zones which suffer from significant triggering effects due to nearby faulting. Thus, although time or slip predictability may hold for a limited window in time or space, this model suggests that it cannot hold over long times at any location. We note that patterns of recent events along the Ecuador-Colombia coast provide support for this result [*Kanamori and McNally*, 1982].

7. Summary and Conclusions

We have formulated a simple model for an earthquake which incorporates the new feature of an inhomogeneous stress distribution upon the fault. This model is based upon techniques developed by *Eshelby* [1957] and corresponds well with observed geometry of mainshock-aftershock sequences. Using the model, one can specify the stress-slip constitutive law and apply either constant far-field displacement or constant far-field stress to the fault. In this way, sequences of earthquakes can be generated.

As a simple first experiment we have chosen a Mohr-Coulomb failure criterion for a two-part fault model. We find that for this case the kinematics of plate motion govern the average properties of an earthquake cycle. Additionally, it can be easily demonstrated that seismic triggering of adjacent faults is a real effect.

Acknowledgments. This work performed in part at Sandia National Laboratories sponsored in part by the U.S. Department of Energy under contract DE-AC04-76DP00789. This work partially performed while the author was a visiting associate at the Seismological Laboratory, California Institute of Technology.

References

Cohen, S. C., The viscoelastic stiffness model of seismicity, *J. Geophys. Res.*, *83*, 5425–5431, 1978.

Das, S., and K. Aki, Fault planes with barriers: A versatile earthquake model, *J. Geophys. Res.*, *82*, 5658–5670, 1977.

Dieterich, J. H., Modeling of rock friction, 1, Experimental results and constitutive equations, *J. Geophys. Res.*, *84*, 2161–2168, 1979.

Dieterich, J. H., Experimental and model study of fault constitutive properties, in *Solid Earth Geophysics and Geotechnology, AMD Symp. Ser.*, vol. 42, edited S. Nemat-Nasser, American Society of Mechanical Engineers, New York, 1980.

Dieterich, J. H., Constitutive properteis of faults with simulated gouge, in *Mechanical Behavior of Crustal Rocks, Geophys. Monogr. Ser.*, vol. 24, edited by N. L. Carter, M. Friedman, J. M. Logan, and D. W. Sterns, pp. 103–120, AGU, Washington, D. C., 1981.

Dmoska, R., and V. C. Li, A mechanical model of precursory source processes for some large earthquakes, *Geophys. Res. Lett.*, *9*, 393–396, 1982.

Ebel, J., and D. V. Helmberger, *P* wave complexity and fault asperities: The Borrego mountain earthquake of 1968, *Bull. Seismol. Soc. Am.*, *72*, 413–438, 1982.

Eshelby, J. D., The determination of the elastic field of an ellipsoidal inclusion and related problems, *Proc. R. Soc. London Ser. A*, *241*, 376–396, 1957.

Hartzel, S., and D. V. Helmberger, Strong-motion modeling of the Imperial Valley earthquake of 1979, *Bull. Seismol. Soc. Am.*, *72*, 571–596, 1982.

Kagan, Y., and L. Knopoff, Statistical search for non-random features of the seismicity of strong earthquakes, *Phys. Earth Planet. Inter.*, *12*, 291–318, 1976.

Kanamori, H., The nature of seismicity patterns before major earthquakes, in *Earthquake Prediction, An International Review, Maurice Ewing Ser.*, vol. 4, edited by D. W. Simpson and P. G. Richards, pp. 1–19, AGU, Washington, D. C., 1981.

Kanamori, H., and K. C. McNally, Variable rupture mode of the subduction zone along the Ecuador-Colombia coast, *Bull. Seismol. Soc. Am.*, *72*, 1241–1253, 1982.

Kellogg, O. D., *Foundations of Potential Theory*, Springer-Verlag, New York, 1929.

Lay, T., H. Kanamori, and L. Ruff, The asperity model and the nature of large subduction zone earthquakes, *Earthquake Predict. Res.*, *1*, 3–71, 1982.

McGarr, A., Analysis of peak ground motion in terms of a model of inhomogeneous faulting, *J. Geophys. Res.*, *86*, 3901–3912, 1981.

McNally, K., and J. B. Minster, Nonuniform seismic slip rates along the middle America Trench, *J. Geophys. Res.*, *86*, 4949–4959, 1981.

Minster, J. B., and T. H. Jordan, Present-day plate motions, *J. Geophys. Res.*, *83*, 5331–5354, 1978.

Mogi, K., Migration of seismic activity, *Bull. Earthquake Res. Inst. Tokyo Univ.*, *46*, 53–74, 1968*a*.

Mogi, K., Development of aftershock area of great earthquakes, *Bull. Earthquake Res. Inst. Tokyo Univ.*, *46*, 175–293, 1968*b*.

Mogi, K., Seismic activity and earthquake prediction, in *Proceedings of the Symposium on Earthquake Prediction Research*, pp. 203–214, Seismological Society of Japan, Tokyo, 1977.

Rice, J. R., Theory of precursory processes in the inception of earthquake rupture, *Gerlands. Beitr. Geophys.*, *88*, 91–127, 1979.

Routh, E. J., *Analytical Statics*, vol. 2, Cambridge University Press, New York, 1892.

Rudnicki, J. W., The inception of faulting in a rock mass with a weakened zone, *J. Geophys. Res.*, *82*, 844–854, 1977.

Rundle, J. B., Viscoelastic crustal deformation by finite, quasi-static sources, *J. Geophys. Res.*, *83*, 5937–5945, 1978.

Savage, J. C., A dislocation model of strain accumulation and release at a subduction zone, *J. Geophys. Res.*, *88*, 4984–4996, 1983.

Savage, J. C., and W. H. Prescott, Asthenosphere readjustment and the earthquake cycle, *J. Geophys. Res.*, *83*, 3369–3376, 1978.

Shimazaki, K., and T. Nakata, Time-predictable recurrence model for large earthquakes, *Geophys. Res. Lett.*, *7*, 279–282, 1980.

Stewart, G. S., E. P. Chael, and K. C. McNally, The November 29, 1978, Oaxaca, Mexico, earthquake: A large, simple event, *J. Geophys. Res.*, *86*, 5053–5060, 1981.

Stuart, W. D., Review of theories for earthquake instabilities, *U.S. Geol. Surv. Open File Rep.*, *78-380*, 541–588, 1978.

Stuart, W. D., Strain softening prior to two-dimensional strike-slip earthquakes, *J. Geophys. Res.*, *84*, 1063–1070, 1979.

Stuart, W. D., and G. Mavko, Earthquake instability on a strike-slip fault, *J. Geophys. Res.*, *84*, 2153–2160, 1979.

Tajima, F., and H. Kanamori, Global variation of expansion pattern of aftershock area, *Eos Trans. AGU*, *62*, 949, 1981.

Thatcher, W., and J. B. Rundle, A model for the earthquake cycle in underthrust zones, *J. Geophys. Res.*, *84*, 5540–5556, 1979.

Thatcher, W., and J. B. Rundle, A viscoelastic coupling model for the cyclic deformation due to periodically repeated earthquakes at subduction zones, *J. Geophys. Res.*, *89*, 7631–7640, 1984.

Thatcher, W., and J. C. Savage, Triggering at large earthquakes by magma chamber inflation, *Geology*, in press, 1983.

Truesdell, C., and W. Noll, *The Nonlinear Field Theories of Mechanics*, Springer-Verlag, New York, 1965.

Vidale, J., and H. Kanamori, The October 1980 earthquake sequence near the New Hebrides, *Geophys. Res. Lett.*, *10*, 1137–1140, 1983.

Walsh, J. B., Stiffness in faulting and in friction experiments, *J. Geophys. Res.*, *76*, 8597–8598, 1971.

Weldon, R. J., and K. E. Sieh, Offset rate and possible timing of recent earthquakes on the San Andreas fault in Cajon Pass, California, *Eos Trans. AGU*, *62*, 1048, 1981.

H. Kanamori, California Institute of Technology, Pasadena, CA 91125.

K. C. McNally, University of California, Santa Cruz, CA 95064.

J. B. Rundle, Sandia National Laboratories, Albuquerque, NM 87185.

(Received June 23, 1983;
revised July 20, 1984;
accepted July 23, 1984.)